MULTICOLOUR OPTICAL PHOTOMETRY OF ACTIVE GEOSTATIONARY SATELLITES

Andrew Jolley*
Defence Space Coordinating Office, Canberra, Australia
Donald Bédard†, Gregg A. Wade‡
Royal Military College of Canada, Kingston, Canada

Abstract

Although broadband photometry has been used to infer information about artificial satellites since soon after the launch of Sputnik 1, the development of photometric techniques for unresolved space object identification or characterisation has been hampered by the large number of variables involved. Many individual studies, and some long ongoing experiments, have used costly metre-class telescopes to obtain data despite other experiments demonstrating that much more flexible and affordable small aperture telescopes may be suitable for the task. In addition, due to the highly time consuming and weather dependent nature of obtaining photometric observations, many studies have suffered from limited data sets, or relied upon simulations to support their claims. With this in mind, an experiment was conducted with the aim of determining the utility of small aperture telescopes for conducting broadband multicolour photometry of satellites for the purpose of unresolved space object identification and characterisation. A 14 inch Celestron CG-14 telescope was used to gain multiple night-long, high temporal resolution data sets of six active geostationary satellites. The results of the experiment cast doubt on the efficacy of some of the previous approaches to obtaining and analysing photometric data. It was discovered that geostationary satellite lightcurves can vary to a greater degree than has generally been recognised, and colour ratios vary considerably with changes in the illumination/observation geometry, making it difficult to use colour for satellite discrimination. Evidence of variations in the spectral energy distribution of sunlight reflected off satellite surface materials was also obtained, which could have implications for surface material identification and techniques that aim to separate satellite body and solar panel contributions to the total observed spectra.

1 INTRODUCTION

Significant progress has been reported over the last decade regarding the potential for photometry to reveal details about artificial Earth orbiting objects [1–4]. Substantial effort has been invested into satellite discrimination and health status determination, as well as characterising resident space objects (RSOs) in terms of their size, mass, surface material composition, or area to mass ratio based solely on measurements of the intensity of reflected light [4–9]. Of note, however, is that much of the photometric analysis conducted to date has suffered from limitations in the data sets. Examples of these limitations include: data being obtained on very few different nights, low temporal resolution, and large gaps in lightcurve data. As a result, questions remain as to how well all possible variables have been considered in the analysis of reflected intensities. For example, Bédard has demonstrated that the sun/object/sensor geometry associated with the instantaneous photometric or spectrometric signature of a satellite is probably far more important than has previously been assumed [10, 11]. Whilst the longitude dependent phase angle has been used extensively to compare photometric signatures, the specific orientation of the satellite has not always been considered. Therefore, it was decided that it was necessary to return to first principles and collect high cadence, long period observations (i.e. over the course of an entire night) on a limited number of geostationary (GEO) satellites, over as many nights as possible. This approach was taken to minimise the chance of under-sampling impacting upon the

*Squadron Leader, Royal Australian Air Force, andrew.jolley@defence.gov.au
†Major, Assistant Professor, Department of Physics, donald.bedard@rmc.ca
‡Professor, Head of the Department of Physics, gregg.wade@rmc.ca

analysis of the data obtained. Advantages of geostationary satellites, in relation to this experiment, include the fact that they can be observed for an entire night through an unchanging airmass, and they usually employ three-axis stabilisation, which constrains their orientation relative to the observer.

This work represents a brief summary of the principle results derived during this investigation. A detailed report is provided by Jolley (2014) [12].

2 EXPERIMENT SETUP AND PROCEDURE

Throughout the experiment, observations were taken using a 14 inch Celestron CG-14 telescope fitted with an Apogee Alta U42 camera. The telescope is mounted on a Paramount ME mount, and includes a temperature compensating focusser and a five slot filter wheel. Standard Bessel BVRI filters were used in the filter wheel [13]. The entire telescope and camera setup was housed in a dome on the roof of one of the academic buildings at the Royal Military College of Canada in Kingston, Canada.

The Apogee Alta U42 has a 2048 x 2048 pixel CCD and uses 16 bit digitisation. The camera, telescope and dome are controlled remotely from a computer in the Space Surveillance Research Laboratory (SSRL), operating The Sky X Pro, CCDSoft 5, Automadome, and Orchestrate for automation, all by Software Bisque.

2.1 DATA ACQUISITION

Twelve nights of observations were conducted, excluding nights where the data obtained were not of sufficiently high quality, on six GEO satellites from 27 July 2013 through to 20 November 2013. Since all of the imaged satellites were part of GEO clusters, each image contained more than one satellite on all except for two nights. As a result, every satellite was imaged on between three and eight nights. Table 1 details the satellites that were observed and the number of nights of imagery obtained for each. The satellites in GEO cluster number 1 are all located at longitude 55.5° West [14], and the satellites in GEO cluster number 2 are all located at longitude 107.3° West [15].

GEO Cluster 1		
Satellite	**Bus Type**	**Nights Imaged**
Galaxy 11	BSS702C	8
Intelsat 805	AS-7000	6
GEO Cluster 2		
Satellite	**Bus Type**	**Nights Imaged**
Anik F1	BSS702C	4
Anik F1R	Eurostar-3000S	4
Anik G1	LS-1300	4
Echostar 17	LS-1300	3

Table 1: Number of nights that each satellite was observed.

In selecting the nights on which to conduct observations, the primary criterion was that the sky should be forecast to be completely clear of cloud until after sunrise. This decision was made because the experimental setup did not include an infrared camera capable of showing the presence of clouds, and therefore doubt could otherwise arise as to whether variations in satellite brightness were the result of clouds or true variations in the signal. Consideration was also given to phases of the Moon and the proximity of the Moon to the satellites being imaged. One night's data were discarded entirely because the nearly full Moon passed sufficiently close to the satellite being imaged to significantly affect the measurements.

Each night, before imaging the satellites of interest, 10 twilight flats were taken through each filter, followed by 25 bias frames and 10 dark frames of 1 minute duration, which is at least as long as each of the data frames. Median master frames were later produced from the multiple bias, dark and flat images. In addition to the bias, dark, and flat frames, images of Landolt standard star fields were taken either at the start or end of the night to enable the calibration of instrumental magnitudes to the standard apparent magnitude scale.

Once the Landolt star images were obtained the telescope was slewed to the GEO cluster of interest, and the data images were taken with sidereal tracking turned off. The imaging sequence was programmed into Orchestrate, which was used to automate the process of cycling through the filters and taking images at the desired exposure time. Only one image was taken through each filter before changing to the next filter. Although Orchestrate significantly reduced the effort required to obtain the data, it remained necessary to closely monitor the images as each one was obtained, due to the rapid changes in brightness that were commonly encountered during satellite observations. Figure 1, for example, shows how quickly satellites can increase in brightness during specular glints.

(a) Image showing all four satellites not saturating the CCD.

(b) Image showing Echostar 17 (bottom of image) saturating the CCD.

Figure 1: Two consecutive images taken through the V filter on 12 Oct 2013 that demonstrate how rapidly satellites can increase in brightness. Both images show satellite cluster two, with Anik F1, F1R, and G1 at the top of the image, and Echostar 17 at the bottom of the image. The image on the left used a 20 second exposure, and the image on the right was taken using a 3 second exposure, after first cycling through the other filters. The image on the right shows Echostar 17 now significantly saturating the CCD less than 2 minutes after the image on the left was taken, despite the reduction in exposure time.

Throughout each night a signal level of between 10000 ADU and 50000 ADU was attempted to be maintained for the brightest pixel illuminated by the satellites being observed. When the brightness was seen to increase markedly it was necessary to reduce the exposure time to avoid saturating any of the pixels; and when the brightness decreased the exposure times were increased to maintain sufficiently high SNRs. This effort was made significantly more complicated whenever more than one satellite was being observed in each frame, which occurred on all except for two nights. In these cases the satellites in the frame often showed significant differences in brightness. Whilst great effort was made to maintain each satellite's measured signal between the limits stated above, sometimes it was not possible to do so. When this occurred, one satellite was selected to be the primary satellite of interest. The primary satellite was always maintained within the signal limits, which occasionally resulted in either saturated pixels or low SNR for the other satellites. Any satellite observations containing saturated pixels or excessively low SNR were later discarded.

Typically, exposure times at the beginning of a night were as follows: 45 to 60 seconds for the B filter, 20 to 30 seconds for the V filter, 5 to 15 seconds for the R and I filters, and 2 to 5 seconds for the unfiltered case. The exposure times usually only decreased minimally until just prior to the main specular glint, when they would quickly drop to less than one second in each filter. After the specular glint the exposure times

were returned to values similar to those used at the start of the night. On nights when the main specular glint was not particularly bright the exposure times for all filters never dropped below approximately 1 to 5 seconds for all filters.

Image processing was conducted using Mirametrics' Windows based Mira Pro Ultimate Edition software program (Mira Pro UE). The image reduction procedure involved subtracting master bias and dark frames and applying flat field corrections to the data images. Instrumental magnitudes were calculated by using Mira's aperture tool that measures the ADU count within a circular synthetic aperture. Landolt star fields were used to calculate the nightly zero point, which was added to each satellite's measured instrumental magnitude to arrive at the apparent magnitude. All magnitude data were exported from Mira to Microsoft Excel, and then input to Matlab for plotting.

For each of the satellites that were observed, lightcurves were constructed for each of the filter bands, and for the unfiltered data, on each night that observations were taken. The lightcurves for the data obtained using filters depict apparent magnitudes, whereas the lightcurves produced from unfiltered observations depict instrumental magnitudes since there exists no standard photometric system specific to unfiltered data obtained using the particular equipment used in this experiment. Each lightcurve consists of approximately 200 data points. Throughout this experiment, time (represented as minutes since midnight UTC) is placed on the horizontal axis for all plots, rather than phase angle. The primary reason for doing so is to simplify the process of reconstructing the sun-satellite-sensor geometry should a reader want to do so.

In general, the most prominent feature of each lightcurve was a short period of brightening lasting for approximately one hour, consistent with the description of glints that have frequently been reported as due to specular reflections off satellite solar arrays [16–19]. The precise shape of the curve during these periods of brightening varied between the different satellites, and sometimes there was more than one peak visible. In addition, the degree of brightening changed for each satellite from one night to another, varying between about one magnitude and ten magnitudes above the level outside of the specular glint.

In addition to the lightcurves, six different colour index plots were constructed for each satellite. The colour indicies that were considered are B-V, B-R, B-I, V-R, V-I, and R-I. Rather than each satellite's colours remaining constant throughout a given night, there was often significant variability. In addition, the shape of a given satellite's colour index plot often varied from one night to another.

3 DISCUSSION

3.1 EXAMINATION OF THE CONCEPT OF LIGHTCURVE CLASSES

One of the more fundamental, and widely accepted, proposals regarding satellite characterisation is that each satellite can be classified into one of five groups (classes) according to the shape of their lightcurves: Canonical, BSS702C, Telstar, A2100, or Peculiar [2, 17, 19–21]. Although it is understood that a particular satellite's glints will vary in magnitude at different times of the year, it is commonly expected that the overall lightcurve class will remain the same because it has been concluded that satellite lightcurves are tightly correlated with their basic bus structure [17]. There have occasionally been results published, however, that cast doubt on this conclusion. It has been noted that, to avoid lightcurve mischaracterisation, seasonal lightcurve variations should be considered [20]. Also, some measured lightcurves have differed greatly from their expected shapes based upon the satellite bus structure [19]. A lack of data seems to have prevented a thorough analysis of the consistency of satellite lightcurve shapes, considering their seasonal variations throughout the year.

Although some of the lightcurve sets produced during this experiment exhibit similar shapes for a given satellite, such as can be seen in Figure 2, there were several examples where a given satellite's lightcurve shape varied considerably over time.

Galaxy 11 was imaged on eight nights over a period of time exceeding two months. Although this only represents less than one fifth of a year, the lightcurve seems to evolve over time in an interesting, and arguably unpredictable way. There are three main features of the Galaxy 11 lightcurves, depicted in Figure 3, that change considerably over the two months.

There are two relatively smooth glint features centred at approximately 200 and 260 minutes since midnight, and one glint feature centred near 370 minutes since midnight that has a much more noisy appearance. The intensities of the two smooth glint features, above the base magnitude level, appear to maintain the same ratio as they vary from one night to another. They also seem to have an inverse relationship to the size of the noisy glint feature. Galaxy 11's lightcurve has been described as belonging to the Peculiar class, rather

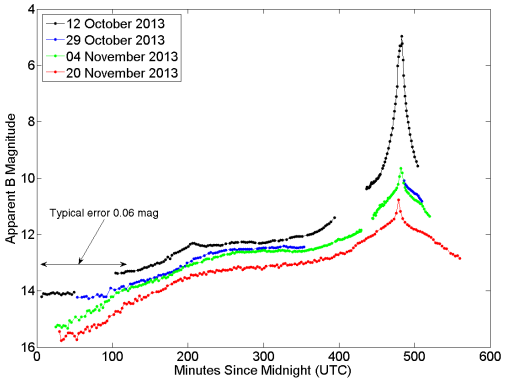

(a) Anik G1 B Band Lightcurve.

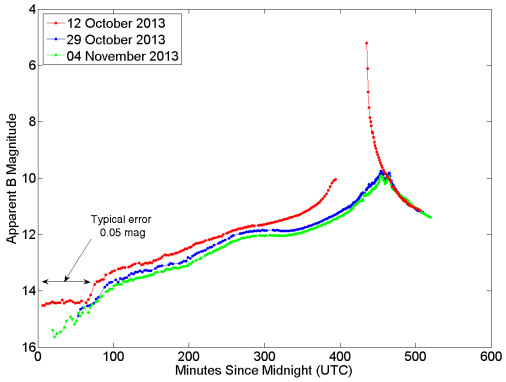

(b) Echostar17 B Band Lightcurve.

Figure 2: B Band Lightcurves for Anik G1 (a), and Echostar 17 (b).

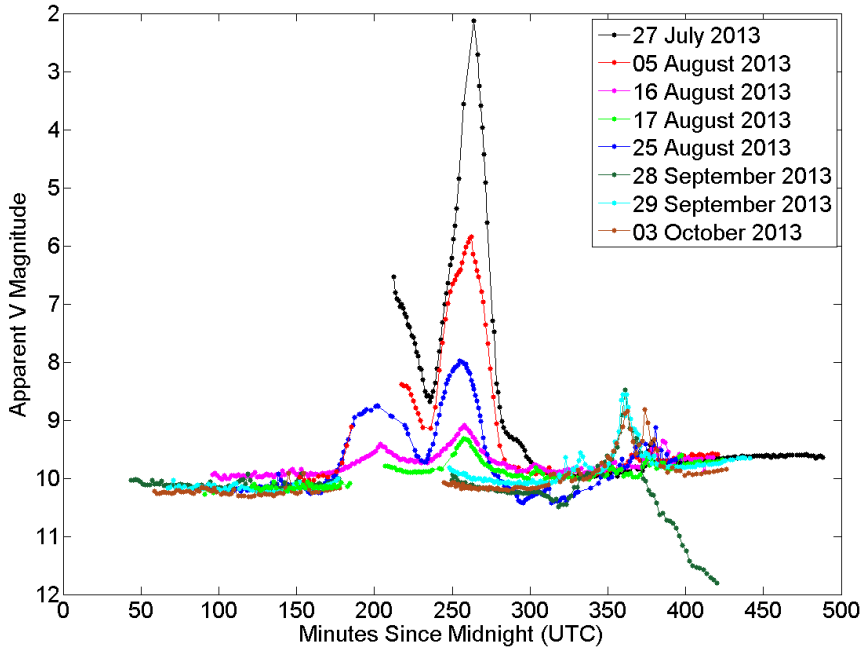

Figure 3: Galaxy 11 V Band Lightcurve.

than the BSS702C class despite it having a BSS702C bus, and also despite the assertion that lightcurve classifications are strongly correlated to basic bus type [17]. Figure 3 would seem to support classifying Galaxy 11's lightcurve as Peculiar, casting doubt on the degree of correlation between bus type and lightcurve class. Furthermore, when Galaxy 11's lightcurves are separated into individual plots for nights that are within one week of each other, as illustrated in Figure 4, the appropriate classification becomes less clear.

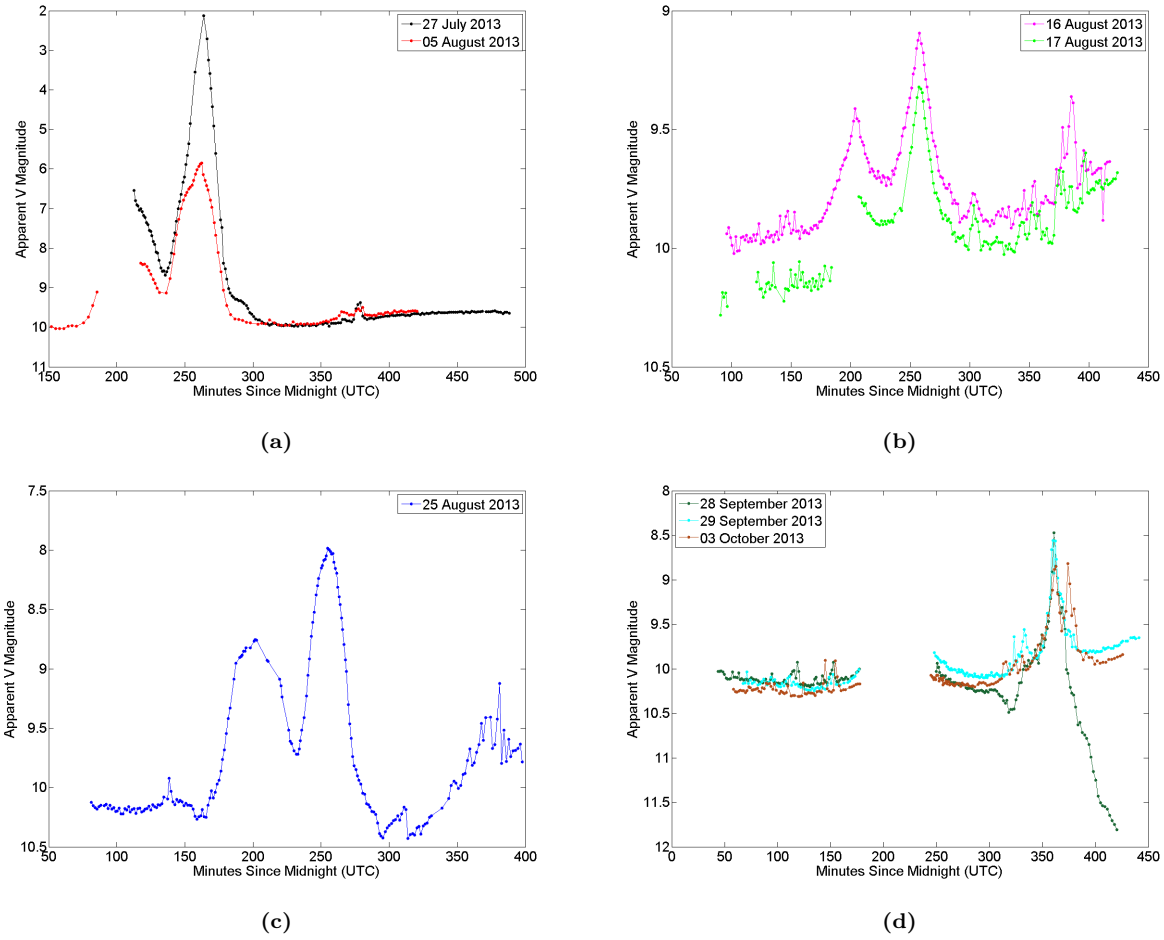

Figure 4: Galaxy 11 V Band lightcurves plotted on separate axes. Lightcurves with similar shapes are plotted together. The gaps in the data evident on the 05th and 17th of August are due to technical difficulties, and the gaps in the data in Figure 4d are due to the satellite passing through Earth's shadow.

Close inspection of Figure 4b reveals three smooth specular peaks, roughly evenly spaced in time but with greatly different amplitudes, centred near zero phase angle, which occurs at 214 minutes since midnight. These lightcurves would seem to be most similar to the Telstar category, although the secondary peaks are offset from the primary peak by much less than 40 degrees phase angle, and beyond about 320 minutes since midnight variations in the lightcurve take on a much more noisy appearance. Thus, the lightcurve might also be described as belonging to the Peculiar category. Examination of Figures 4a and 4c reveals smoothly varying lightcurves with two specular peaks. There are no data for the 27th of July prior to 215 minutes since midnight because of the late sunset experienced during summer so it cannot be guaranteed that there are no more peaks prior to that time. There are no further peaks prior to that time apparent in the 05th and 25th of August data, however. None of the defined lightcurve classes perfectly describes these plots, however the most closely matching description is that of the A2100 class, which is characterised by two smooth peaks showing general but imperfect symmetry around a local minima near zero degrees phase angle [17]. Finally, Figure 4d displays a completely different shape again. Where the primary specular peak is present in the

other figures, near 260 minutes since midnight, there is no evidence of a glint at all. It does appear as though the eclipse period may have masked a broad peak that would have otherwise appeared near the one centred at 200 minutes since midnight in the other plots; however it is difficult to know exactly what shape the peak would have. Also, the most prominent feature, present near 370 minutes since midnight, is located where there is relatively little or no discernable feature in the other nights' plots. Figure 4d is not symmetrical or smoothly varying, and could therefore best be classified as Peculiar.

Noting that these lightcurves only span a period of approximately two months, the fact that they might be classified in at least three different ways during this period indicates that a particular lightcurve class cannot be assigned uniquely to Galaxy 11, and that the appropriate lightcurve class is not tightly correlated to the satellite bus type.

Intelsat 805, based upon the AS-7000 bus [22], also arguably can be categorised according to more than one specific lightcurve class. Figure 5 depicts the V band Intelsat 805 lightcurves. Figure 5a shows the two lightcurves for mid-August, and Figure 5c the curve for late August. The gap in the 25 August curve is due to obstruction by clouds. The most appropriate classification based upon these curves is not entirely clear, however there is a peak near zero phase angle, which occurs at 214 minutes since midnight, and two slightly asymmetric smaller peaks either side of the primary peak. The peak that occurs at the start of the night is not entirely covered by the 16th and 17th of August curves. It would therefore appear that the Telstar class would be the most appropriate based on Figure 5a.

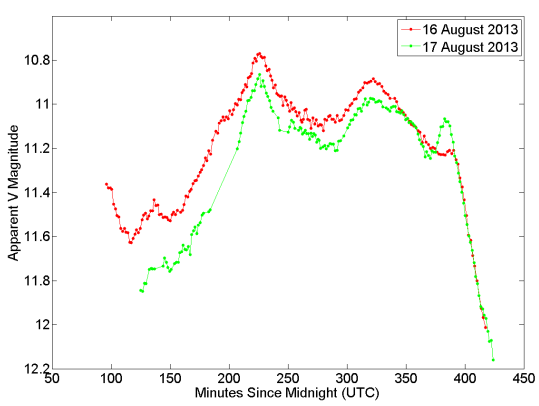

(a) Intelsat 805 V Band Lightcurve.

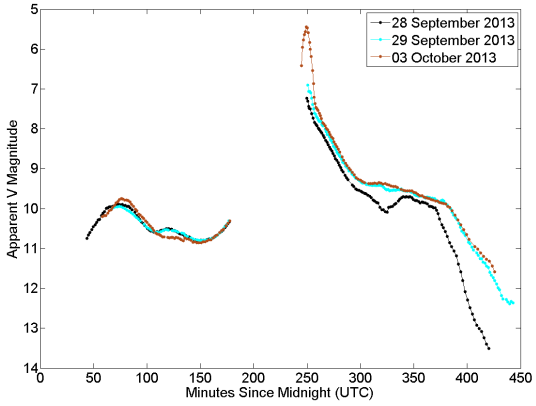

(b) Intelsat 805 V Band Lightcurve.

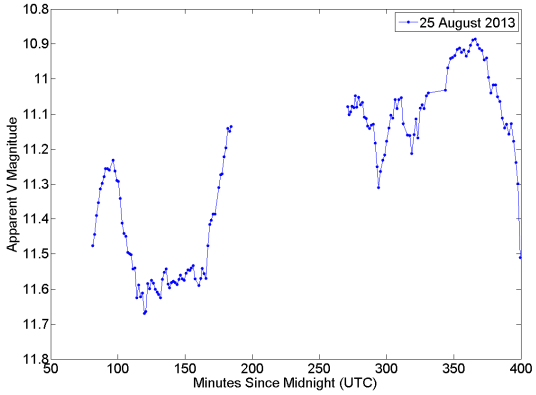

(c) Intelsat 805 V Band Lightcurve.

Figure 5: Intelsat 805 V Band lightcurves on separate axes.

In contrast, Figure 5b, depicting lightcurves for late September and early October, is much more asymmetric. The gaps in the data are due to the satellite passing into eclipse. Given the lack of symmetry, these curves would likely be classified as Peculiar.

Observations of both Galaxy 11 and Intelsat 805 occurred over a period of less than ten weeks. Despite this, each satellite produced more than one type of lightcurve class. In addition, the satellites' lightcurve

classes do not necessarily seem to be very well correllated to their bus type. Although more data is required, ideally gathered over many nights throughout an entire year, it is clear that lightcurve shapes of individual satellites can change fundamentally with time. It seems likely that lightcurve classes are not a very effective tool for grouping or classifying satellites. At the very least lightcurve classes would be specific to a particular period of time in at least some cases.

3.2 VARIATION OF SPECTRAL ENERGY DISTRIBUTION

The invariance of a given material's SED is a key assumption that is fundamental to many proposed advances in the use of multicolour photometry for SSA [9, 21, 23–27]. Bédard has presented evidence to suggest that this assumption is actually incorrect [28, 29]. The data collected during this experiment were analysed for evidence that supports or contradicts the assumption of invariable SED.

Examination of each satellite's colour plots near the brightest specular peaks reveals one interesting detail in particular. Each specular peak coincides with a change in colour ratio for every colour plot, for all of the satellites. The brightest specular reflections, however, exhibit a reversal in the colour ratio change, over a short timeframe, at the peak. Intelsat 805 provides a clear illustration of this phenomenon. Figure 6 depicts Intelsat 805's B band lightcurves above the B-R colour variations.

The most striking feature of the colour plot is the dramatic increase in the relative intensity of the shorter wavelengths between 250 and 300 minutes since midnight on the 28^{th} and 29^{th} of September, and the 3^{rd} of October. Unfortunately, a significant gap in the data exists on these nights due to the satellite being eclipsed by Earth's shadow. The peak in the lightcurve was captured on the 3^{rd} of October, and very narrowly missed during the September observations. By comparison to the B band lightcurve it is clear that the change in colour ratio begins to occur at the base of the specular peak, and that the colour becomes increasingly blue as the lightcurve magnitude increases. Within approximately 15 minutes of the peak, however, the colour reddens sharply to reach close to the same colour ratio as existed prior to the specular glint.

It is widely believed that the bright peaks common to most GEO satellite's lightcurves are caused by specular reflections off their solar panels, and there is much evidence to suggest this is correct. It seems intuitive that a dramatic increase in the solar panel's contribution to the overall intensity would lead to a more blue colour ratio because solar panels usually appear blue to the naked eye. The sudden reddening near the peak, however, is not consistent with this reasoning. We propose three possible causes for the colour ratio reversal:

1. A second specular reflection, off a facet other than the solar array, is being observed;
2. The relative increase in intensity at longer wavelengths is due to the SED of light reflected off the solar array changing with the illumination-observation geometry; or
3. A combination of both of the first two explanations.

If the first explanation is the correct one, then the plane of the facet causing the reddening must be very closely aligned with the plane of the solar array because the local maxima near 250 minutes since midnight on the colour plot coincides with the specular peak on the lightcurve. Also, the cone of specular reflection off the second facet must be narrower (more mirror-like) than off the solar array because the reddening occurs over a shorter time interval than the increase in blue due to the solar panels. In addition, very close to the specular peak, the increase in intensity at the red end of the spectrum occurs more steeply with time than the increase in intensity at the blue end of the spectrum. Therefore, the facet causing the reddening must be either larger than the solar array or exhibit much greater reflected flux at longer wavelengths than shorter wavelengths. As depicted in Figure 7 there are no facets larger than the solar array on Intelsat 805, as is common amongst GEO satellites [22]. Also, the satellite is stabilised such that the antennas always point towards Earth. Therefore, Figure 7 would seem to indicate that the gold coloured MLI, which is known to be relatively red [29], does not present a significant flat surface towards Earth that might be capable of producing a bright specular reflection to rival that of the solar array.

It seems unlikely that the colour ratio variation across the primary specular peak could be due to satellite components other than the solar panels. The alternative explanation, that it is due to the SED varying with changing illumination-observation geometry, fits more easily with observations made during this experiment, and matches the conclusions drawn from Bédard's laboratory work [10, 11]. Figure 8 shows how colour ratios

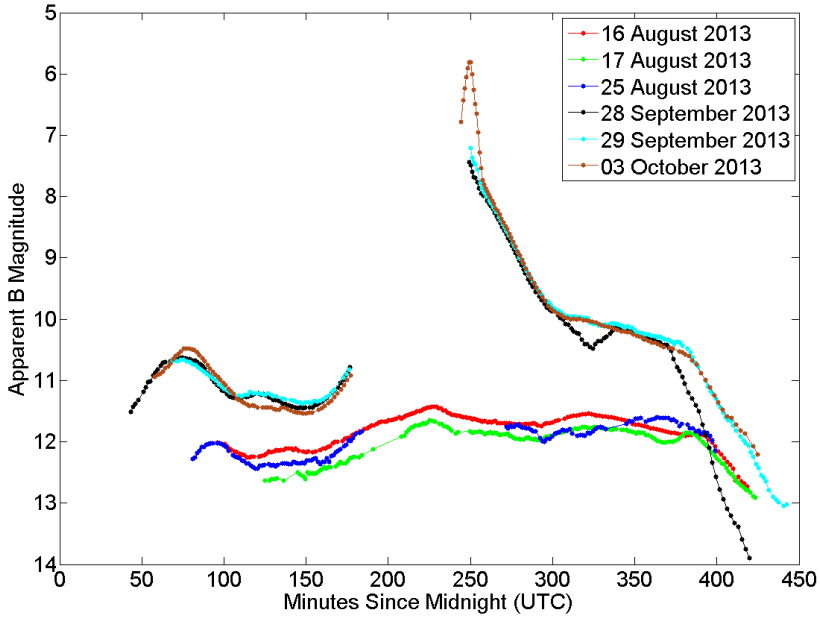

(a) Intelsat 805 B Band Lightcurve.

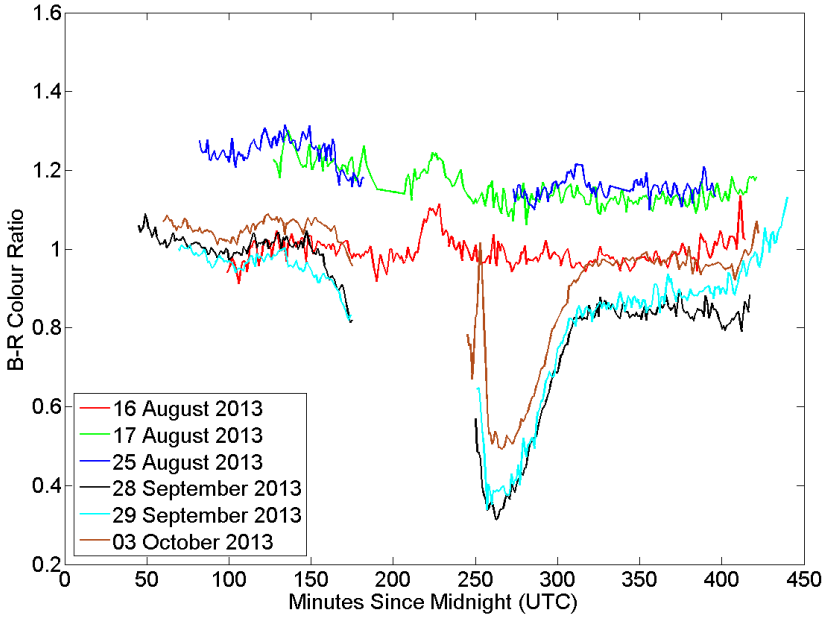

(b) Intelsat 805 B-R Colour Variation.

Figure 6: B Band Lightcurve for Intelsat 805 (a), compared with its B-R colour variation (b).

Figure 7: Artist's depiction of Intelsat 805 [22].

of one particular TJPV solar cell change with observation angle, at a constant illumination angle of 10° [29]. Although the plots only display a range of observation angles of less than two degrees, it is clear that outside of the very narrow cone of specular reflection the colour ratios become sharply more blue. At the specular peak, the B-R colour ratio value is close to unity, as in our observations of Intelsat 805.

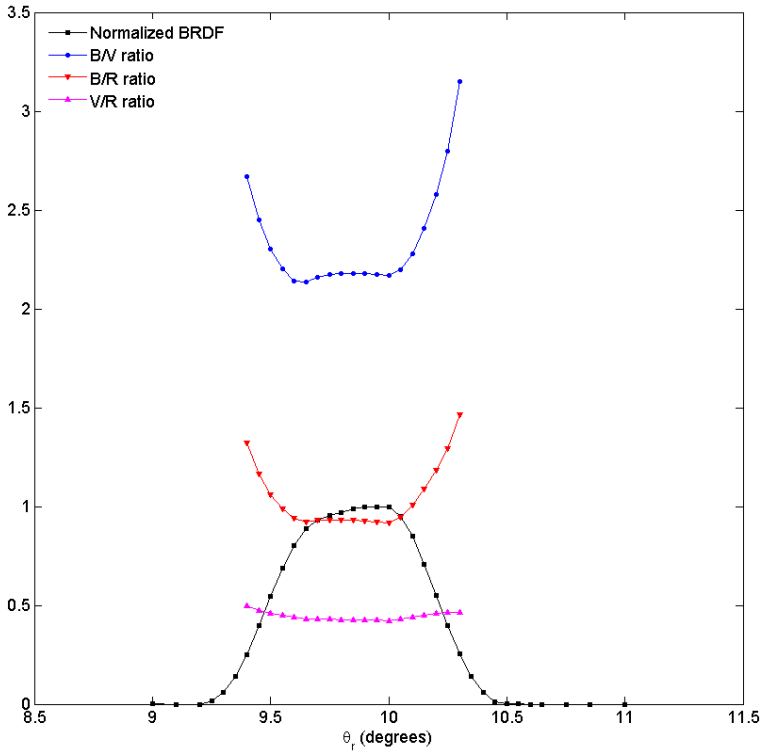

Figure 8: Normalised broadband BRDF measurement and colour ratios of a TJPV cell for varying observation angle (θ_r) at constant illumination angle of 10° [29].

Although the Intelsat 805 solar array is likely to use different solar panels to the one corresponding to Figure 8, all of the four solar cells tested by Bédard yielded similar results. If the cause of the reversal in Intelsat 805's colour ratio change is varying SED, and if the satellite's solar array has similar reflectance properties to that measured by Bédard in Figure 8, then the evolution of the B-R colour ratio with observation angle might be explained as follows:

- At all times the solar panels track the sun, thus maintaining a constant illumination angle of close to

zero;

- At the edge of the primary glint feature the observation angle is such that the specular reflection off the solar array is just beginning to become visible.
- As the observation angle decreases, the contribution from the solar array to the total measured flux increases markedly. Because the SED of the light reflected off the solar array is relatively more blue at these observation angles, the overall colour ratio of the satellite becomes steadily more blue.
- When the observation angle decreases further, to within approximately two degrees of the centre of the cone of specular reflection, the SED abruptly becomes more evenly distributed across the visible spectrum. With a B-R colour ratio close to 1, as in Figure 8, the satellite's total B-R colour ratio returns to a value similar to those measured prior to the specular reflection, as seen with Intelsat 805 in Figure 6b.
- After the observation angle passes beyond the centre of the cone of specular reflection, the colour ratio evolves in the reverse of the manner just described.

The colour ratio reversal feature has also been observed in Anik F1, Anik G1, and Echostar 17 to varying degrees. In Figure 9 the feature is most obvious in the 29 October and 04 November plots near 450 minutes since midnight. The reason that the feature is broader than observed in Intelsat 805 may be that Anik F1 displays three separate, closely space specular peaks.

Anik G1 also displays a very sharp reversal in colour ratio, similar to Intelsat 805, centred at approximately 490 minutes since midnight, as can be seen in Figure 10.

The peak of the specular reflection was not observed for Echostar 17 due to shadowing by Earth, however a sharp reversal in the colour ratio change is apparent in the 12 October data, as depicted in Figure 11.

This work is consistent with the results of Bédard's experiment, strongly indicating that the SED of light reflected off a particular material, in this case solar panels, varies with changing illumination-observation geometry, and that the changing SED affects observed colour ratios. This conclusion has significant implications for previous work that has been conducted in the analysis of multicolour photometry of satellites, particularly where the assumption of invariant SED has been expressly fundamental to that work. On the other hand, knowledge of how different materials' SEDs change with observation-illumination geometry may provide new means of enhancing SSA. For example, it has been well demonstrated that examination of a satellite's lightcurve as a function of longitudinal phase angle can reveal the angular offset between the solar panel normal vector and the satellite-sun vector [17]. Such information constrains the solar panel orientation about one of its axes. When observed, the extremely narrow cone of specular reflection within which a material's colour ratio suddenly changes could also potentially place tight constraints on the attitude of a GEO satellite about its East-West axis. The solar array plane can thus be determined in three dimensions rather than just two.

Further examination of Figure 6, in light of the discussion on varying SED, reveals another interesting feature. On the 16^{th} and 17^{th} of August, the primary specular peak is relatively faint. The associated colour plots do not display the colour reversal that was noted on the other nights, and the colour ratio change occurs in the opposite manner. Instead of the colour steadily becoming more blue as the specular peak is approached, a slight reddening is observed. The same colour ratio behaviour was noted by Payne *et al.* in 2007 [4] when the GEO satellite DTV 1R was observed in March and June. In March the colour ratio was observed to become bluer, whereas in June it became redder.

At first glance the Intelsat 805 colour plots for the 16^{th} and 17^{th} of August seem to contradict the discussion about SED variation: increased contribution from the solar array to the total flux reddens the observed reflection, rather than making it more blue. There is, however, one variable of particular importance that changes continuously with the seasons: the illumination angle. Although Intelsat 805's solar panels continuously rotate to track the sun, their axis of rotation remains fixed relative to Earth's equatorial plane; usually close to perpendicular to it. As a result, seasonal changes in solar declination result in variable solar panel illumination angles. On nights when there is a relatively small specular peak observed, usually at or near the solstices, the illumination angle is the greatest. At or near the equinoxes the illumination angle is smallest, and the specular peak is the brightest. The solar panel illumination angle on the 16^{th} and 17^{th} of August was therefore significantly greater than on the 28^{th} and 29^{th} of September, and the 3^{rd} of October.

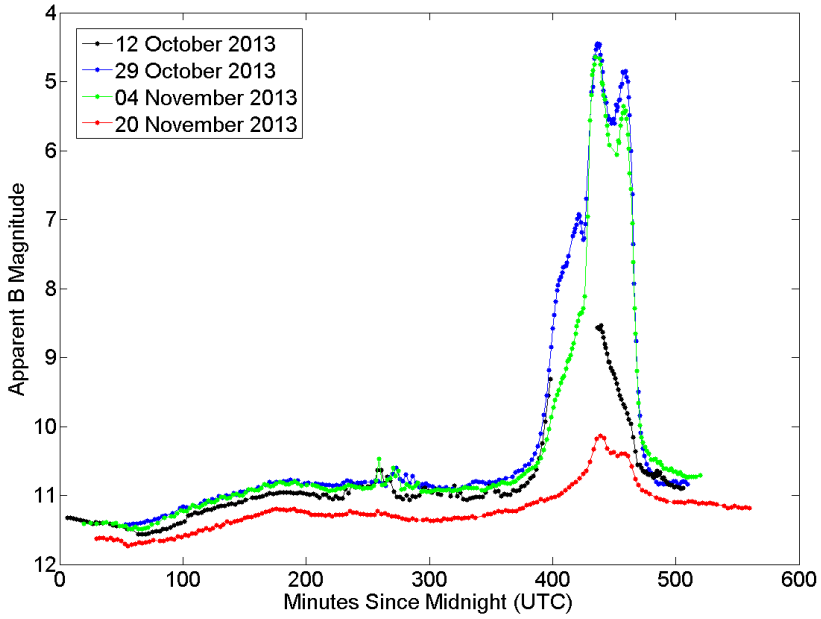

(a) Anik F1 B Band Lightcurve.

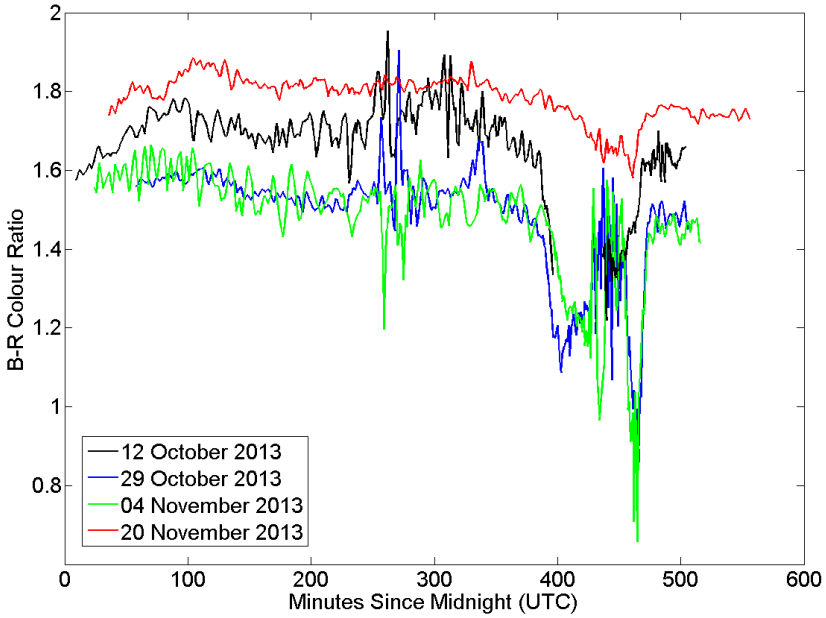

(b) Anik F1 B-R Colour Plot.

Figure 9: B Band Lightcurve for Anik F1 (a), compared with its B-R colour variation (b).

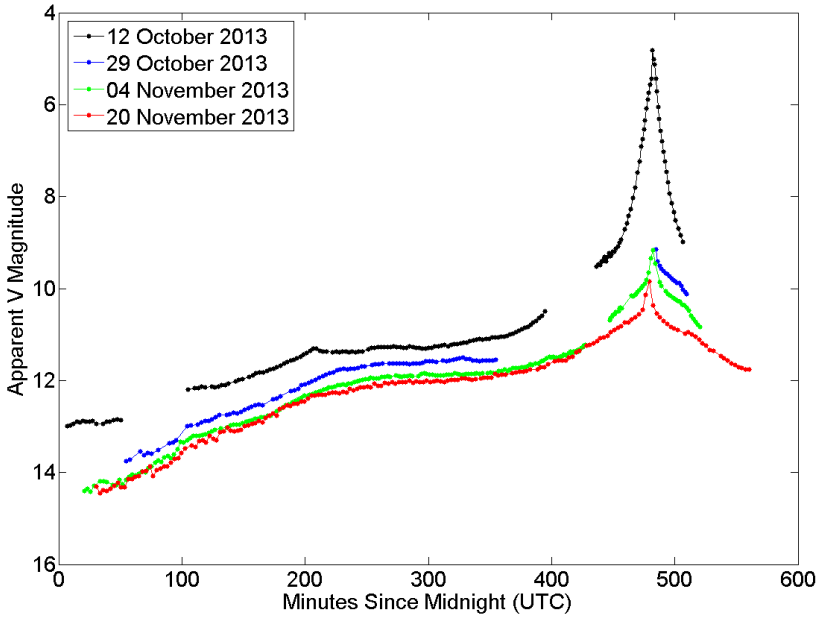

(a) Anik G1 V Band Lightcurve.

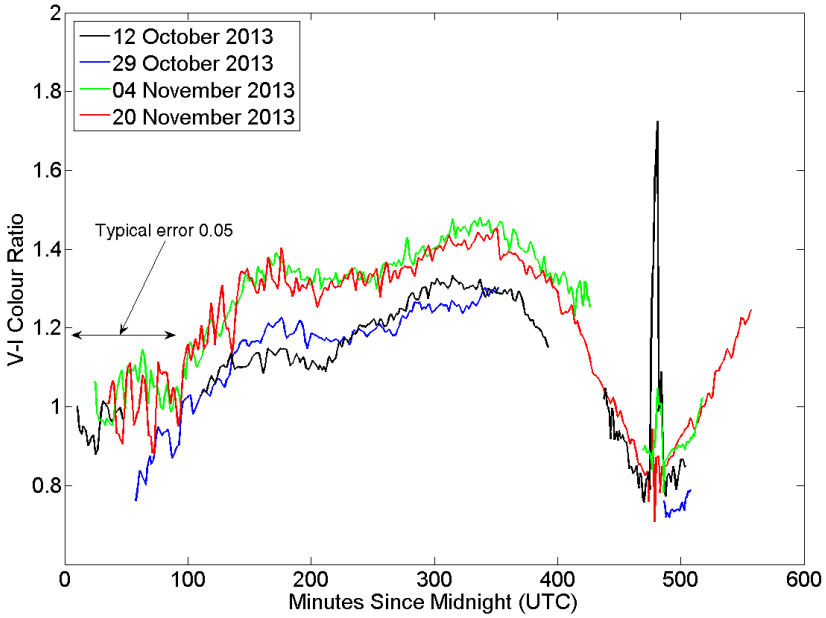

(b) Anik G1 V-I Colour Variation.

Figure 10: V Band Lightcurve for Anik G1 (a), compared with its V-I colour variation (b).

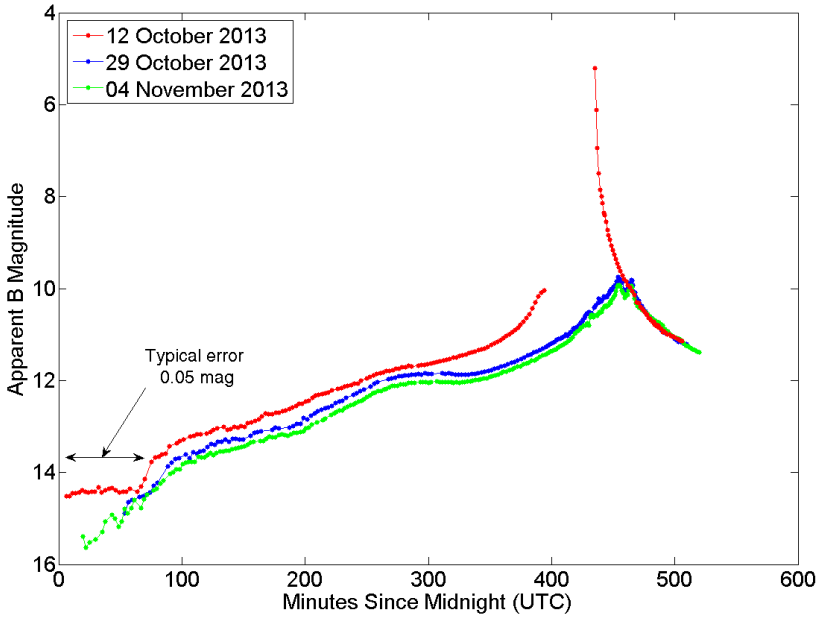

(a) Echostar 17 B Band Lightcurve.

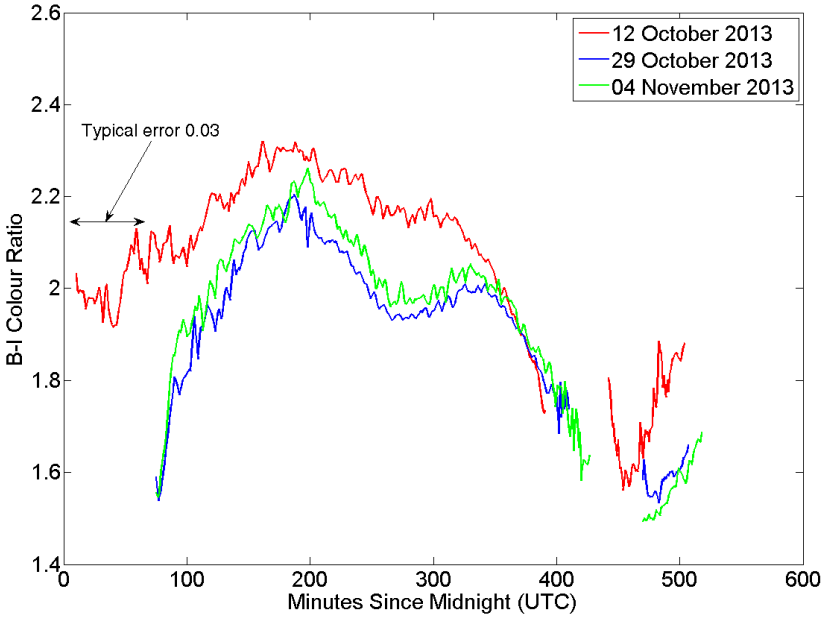

(b) Echostar 17 B-I Colour Variation.

Figure 11: B Band Lightcurve for Echostar 17 (a), compared with its B-I colour variation (b).

At this point, further examination of Bédard's solar panel colour ratio plots is instructive. Figure 12 depicts various colour ratios of the same solar cell referenced in Figure 8, as a function of observation angle, for incidence angles of 30° and 60°.

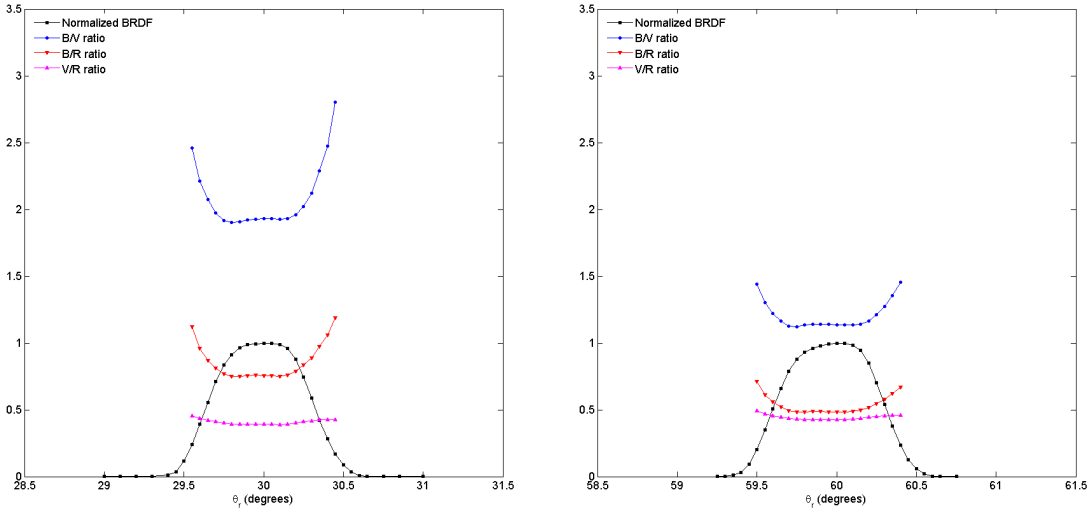

(a) 30° illumination angle. **(b) 60° illumination angle.**

Figure 12: Normalised broadband BRDF measurements and colour ratios of a TJPV cell for varying observation angle (θ_r) at constant illumination angle of 30° (a) and 60° (b) [29].

Of note, the B-R colour ratio in Figure 12b is lower across the entire curve than in Figure 12a, indicating a redder colour. Both of these curves depict redder colour ratios than the B-R curve in Figure 8. What these figures show is that higher illumination angles produce redder colour ratios than lower illumination angles for any given observation angle. At an illumination angle of 60° the observed colour ratio was relatively red across the entire range of observation angles measured by Bédard.

The variable nature of Intelsat 805's B-R colour ratio curves can be explained if the satellite's solar cells have similar reflectance properties to the TJPV cell measured by Bédard. At times of the year near the summer and winter solstices the angle at which the sun's light illuminates a GEO's solar array is the greatest. The specular reflection is thus directed away from Earth's equator; to the north during the northern hemisphere winter, and to the south during the northern hemisphere summer. On the 16$^{\text{th}}$ and 17$^{\text{th}}$ of August the specular reflection off Intelsat 805's solar array was therefore directed away from the observing location in Canada, causing relatively faint glint features. Since the illumination angle was large on those nights, the extra contribution made by the solar panel glint to the measured flux, above the level measured without the specular reflection, consisted of more longer wavelength light than shorter wavelength light. Thus, the overall B-R colour ratio curve exhibits only a slight, brief reddening. These results support Bédard's finding that a material's SED may vary not only with observation angle, but with illumination angle as well.

3.3 THE USE OF COLOUR RATIOS IN SATELLITE DISCRIMINATION AND CHARACTERISATION

A clear implication of these results is that any SSA effort that involves the use of colour ratios can only be applied to space objects whose attitude is accurately known, including the illumination-observation geometry at the time of each observation. This point is illustrated by a study conducted by Payne *et al.* in 2001 [30]. The authors compared magnitude versus colour variations of a cluster of GEOs, using Johnson filters and specially designed Space Object Identification (SOI) In Living Colour (SILC) filters, to conclude that the SILC filters developed by the United States Air Force Research Lab (AFRL) were superior to the Johnson filters for satellite discrimination [30]. Specific details about the timing of the measurements used to construct the magnitude versus colour plots were not provided, however only approximately 12 to 24 measurements were made for each satellite. Figure 13 depicts Anik F1R and Echostar 17 measurements from this experiment, from three nights each, plotted on the same magnitude versus colour plot used by Payne *et al.* It is apparent

that when data collected throughout multiple nights are plotted, it becomes far more difficult to distinguish between different satellites.

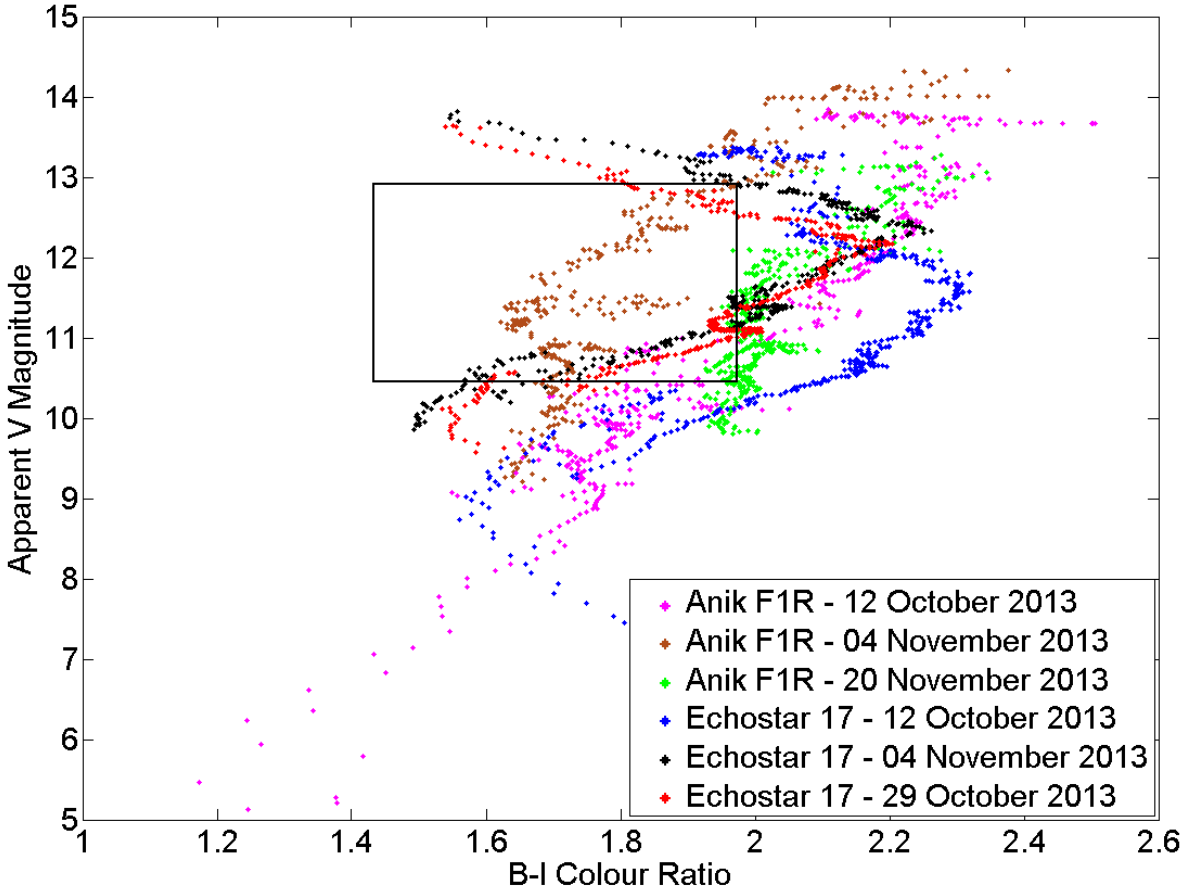

Figure 13: Plot of magnitude vs colour for Anik F1R and Echostar 17. The black rectangle in the centre of the image represents the boundaries within which all of the data from five different satellites plotted by Payne *et al* reside [30].

The data represent measurements taken throughout each night for each satellite. On the 12^{th} of October and the 4^{th} of November the data for each satellite were extracted from the same set of images, and thus represent simultaneous measurements. The black rectangle in the centre of the image represents the boundaries within which all of the data from five different satellites plotted by Payne *et al* reside [30]. Also, Anik F1R and Echostar 17 have significantly different structures. Anik F1R is based upon Astrium's Eurostar 3000S bus, whereas Echostar 17 is based upon the Space Systems Loral SSL-1300 bus [22].

Three things are immediately apparent upon inspecting Figure 13. First, each satellite's data points are not tightly grouped in one small area as might be expected from Payne *et al.*'s analysis of their data. The range of values for each satellite on any of the nights is far greater than the range of values presented for all five of the satellites analysed by Payne together. Second, the location on the plot occupied by each satellite's data points varies significantly from one night to another. Third, there is considerable overlap between the areas on the plot occupied by each satellite. It is clear that it would be impossible to differentiate between Anik F1R and Echostar 17 based upon a small number of measurements plotted on a magnitude versus colour plot, despite the significant differences between their physical structures. In analysing the data obtained throughout this work, the wide variation of magnitude versus colour values exhibited by Anik F1R and Echostar 17 were found to be characteristic of all of the satellites observed.

The observations reported here regarding the variable nature of a given material's SED are important to any photometric study of satellites that relies upon colour ratio measurements. Although it is widely

understood that a satellite's observed colour ratios may change throughout a given night, the factors that influence the colour ratios have not been thoroughly investigated. The current, longstanding, assumption that any material's SED is invariant has led to the conclusion that a satellite's observed colour ratios are purely functions of the materials that are visible and the relative intensity of the light observed to be reflected off each material. For example, a relative increase in red wavelengths is commonly associated with either specular reflections off gold coloured MLI or a greater surface area of MLI becoming visible; whereas a relative increase in blue wavelengths is associated with increased reflection off solar panels. This work has shown that illumination angle and observation angle are both very important factors in determining observed colour ratios: reflections off solar panels may result in either redder or bluer colours.

4 CONCLUSION

This experiment has demonstrated that GEO satellite lightcurves and colour variations do not necessarily behave in a straightforward manner. Spikes in brightness due to specular reflections off solar arrays or parts of the satellite body vary significantly in magnitude throughout the year. The precise sun-satellite-sensor geometry seems to be a critical factor in determining the flux that will be measured by the sensor at a given point in time. As a result, it is often difficult to uniquely classify a satellite by the general shape of its lightcurve, and it appears that a satellite's lightcurve class is not tightly correlated to it's bus type. The illumination and observation geometry also affects the colour ratios that will be measured. In addition, observed colour ratios are significantly influenced by variations in the SED of reflected light, particularly near specular peaks. Far from exhibiting constant colour ratios at all times, each satellite's colours vary considerably throughout a given night. The considerable effect that illumination and observation geometry, and varying SED, has on the observed flux in different bands makes it very difficult to use colour ratios for satellite discrimination.

Because of the number of variables that affect measurements of flux and colour, and the degree to which measurements are affected by small changes in those variables, one must be very careful when making simplifying assumptions about a satellite. Studies that model satellites as simple structures consisting of only two or three basic components cannot capture the effects of small glints off minor satellite surfaces. Similarly, models that do not account for the effect of changing illumination and observation geometry on the SED and intensity of reflected light off each satellite surface risk producing inaccurate results.

5 References

[1] A. Chaudhary, M. Nosek, and B. Klem. Applications of space-based infrared sensor data collections to spacespace health monitoring, space object identification and sensor calibration. In *Proceedings of the 2002 AMOS Technical Conference*, Kihei, Maui, HI, 2002.

[2] A. Chaudhary, T. Payne, S. Gregory, and P. Dao. Fingerprinting of non-resolved three-axis stabilized space objects using a two-facet analytical model. In *Proceedings of the 2011 AMOS Technical Conference*, Kihei, Maui, HI, 2011.

[3] D. Hall, K. Hamada, T. Kelecy, and P. Kervin. Surface material characterization from non-resolved multi-band optical observations. In *Proceedings of the 2012 AMOS Technical Conference*, Kihei, Maui, HI, 2012.

[4] T. E. Payne, S. A. Gregory, J. Tombasco, K. Luu, and L. Durr. Satellite monitoring, change detection and characterization using non-resolved, electro-optical data from a small aperture telescope. In *Proceedings of the 2007 AMOS Technical Conference*, Kihei, Maui, HI, 2007.

[5] P. LeVan. Discrimination of closely space geosynchronous satellites - phase curve analysis & new small business innovative research (sbir) efforts. In *Proceedings of the 2010 AMOS Technical Conference*, Kihei, Maui, HI, 2010.

[6] D. Hall, B. Calef, K. Knox, M. Bolden, and P. Kervin. Separating attitude and shape effects for non-resolved objects. In *Proceedings of the 2007 AMOS Technical Conference*, Kihei, Maui, HI, 2007.

[7] D. Hall. Surface material characterisation from multi-band optical observations. In *Proceedings of the 2010 AMOS Technical Conference*, Kihei, Maui, HI, 2010.

[8] D. Hall. Amos galaxy 15 satellite observations and analysis. In *Proceedings of the 2011 AMOS Technical Conference*, Kihei, Maui, HI, 2011.

[9] K. Jorgensen. *Using Reflectance Spectroscopy to Determine Material Type of Orbital Debris*. PhD thesis, Colorado Centre for Astrodynamics Research, University of Colorado, 2000.

[10] D. Bedard and M. Levesque. Analysis of the canx-1 engineering model spectral reflectance measurements. *Journal of Spacecraft and Rockets*, 51(5):1492–1504, September 2014.

[11] D. Bedard, G. Wade, and K. Abercromby. Laboratory characterisation of homogenous spacecraft materials. *Journal of Spacecraft and Rockets*, pages 1–19, 2015.

[12] A. Jolley. Multicolour optical photometry of active geostationary satellites. Master's thesis, Royal Military College of Canada, 2014.

[13] M. S. Bessel. Ubvri passbands. *Publications of the Astronomical Society of the Pacific*, 102:1181–1199, October 1990.

[14] Intelsat. Satellites and coverage maps, February 2014. URL `www.intelsat.com/infrastructure/satellites-and-coverage-maps`.

[15] Telesat. Telesat - our fleet, February 2014. URL `http://telesat.com/our-fleet#anik-f1`.

[16] T. E. Payne, S. A. Gregory, F. J. Vrba, and K. Luu. Utility of a multi-color photometric database. In *Proceedings of the 2005 AMOS Technical Conference*, Kihei, Maui, HI, 2005.

[17] T. E. Payne, S. A. Gregory, and K. Luu. Ssa analysis of geos photometric signature classifications and solar panel offsets. In *Proceedings of the 2006 AMOS Technical Conference*, Kihei, Maui, HI, 2006.

[18] R. Scott and B. Wallace. Small-aperture optical photometry of canadian geostationary satellites. *Canadian Aeronautics and Space Journal*, 55(2):41–53, 2009.

[19] F. J. Vrba, M. E. DiVittorio, R. B. Hindsley, H. R. Schmitt, J. T. Armstrong, P. D. Shankland, D. J. Hutter, and J. A. Benson. A survey of geosynchronous satellite glints. In *Proceedings of the 2009 AMOS Technical Conference*, Kihei, Maui, HI, 2009.

[20] J. Murray-Krezan, W. Inbody, P. Dao, A. Dentamaro, D. Fulcoly, and S. Gregory. Algorithms for automated characterization of three-axis stabilized geos using non-resolved optical observations. In *Proceedings of the 2012 AMOS Technical Conference*, Kihei, Maui, HI, 2012.

[21] S. A. Gregory, T. E. Payne, and K. Luu. Comparisons between simulated and observed color photometric signatures of geosynchronous satellites. In *Proceedings of the 2005 AMOS Technical Conference*, Kihei, Maui, HI, 2005.

[22] G. Krebs. Gunter's space page, February 2014. URL `www.space.skyrocket.de`.

[23] T. E. Payne, A. Chaudhary, S. Gregory, J. Brown, and M. Nosek. Signature intensity derivative and its application to resident space object typing. In *Proceedings of the 2009 AMOS Technical Conference*, Kihei, Maui, HI, 2009.

[24] K. Abercromby, J. Okada, M. Guyote, K. Hamada, and E. Barker. Comparisons of ground truth and remote spectral measurements of the formosat and ande spacecraft. In *Proceedings of the 2006 AMOS Technical Conference*, 2006.

[25] K. Abercromby, K. Hamada, M. Guyote, J. Okada, and E. Barker. Remote and ground truth spectral measurement comparisons of formosat iii. In *Proceedings of the 2007 AMOS Technical Conference*, 2007.

[26] H. Cowardin, K. Abercromby, E. Barker, P. Seitzer, M. Mulrooney, and T. Schildknecht. An assessment of geo orbital debris photometric properties derived from laboratory-based measurements. In *Proceedings of the 2009 AMOS Technical Conference*, Kihei, Maui, HI, 2009.

[27] S.M. Lederer, P. Seitzer, H.M. Cowardin, E.S. Barker, K.J. Abercromby, and A. Burkhardt. Preliminary characterisation of idcsp spacecrafts through a multi-analytical approach. In *Proceedings of the 2012 AMOS Technical Conference*, Kihei, Maui, HI, 2012.

[28] D. Bedard. Using a physics-based reflectance model to study the reddening effect observed in spectrometric measumeasure of artificial space objects. In *Proceedings of the 2011 AMOS Technical Conference*, Kihei, Maui, HI, 2011.

[29] D. Bedard. *Spectrometric Characterisation of Artificial Earth-Orbiting Objects*. PhD thesis, Royal Military College of Canada, 2013.

[30] T. E. W. Payne, S. A. Gregory, D. J. Sanchez, T. W. Burdillis, and S. A. Storm. Color photometry of geosynchronous satellites using the silc filters. In *Proc. SPIE 4490*, volume 4490, pages 194–199, San Diego, CA, 2001.